Proc. Natl. Acad. Sci. USA
Vol. 91, pp. 836–838, February 1994
Biophysics

Atomic force microscopy produces faithful high-resolution images of protein surfaces in an aqueous environment

(image processing/bacterial cell wall protein)

SIMONE KARRASCH*, REINER HEGERL†, JAN H. HOH*, WOLFGANG BAUMEISTER†, AND ANDREAS ENGEL*

*M. E. Müller-Institute for High-Resolution Electron Microscopy at the Biocenter, University of Basel, Klingelbergstrasse 70, CH-4056 Basel, Switzerland; and †Max-Planck-Institut für Biochemie, D-8033 Martinsried bei München, Germany

Communicated by Calvin F. Quate, October 4, 1993 (received for review July 30, 1993)

ABSTRACT **The atomic force microscope has the potential to monitor structural changes of a biological system in its native environment. To correlate them with the biological function at a molecular level, high lateral and vertical resolution are required. Here we demonstrate that the atomic force microscope is capable of imaging the surface of the hexagonally packed intermediate layer of *Deinococcus radiodurans* in buffer solution with a lateral resolution of 1 nm and a vertical resolution of 0.1 nm. On average, these topographs differ from those determined by electron microscopy by <0.5 nm.**

The atomic force microscope (AFM) (1) moves a sharp tip over a surface to record its topography. This instrument can be used to image biological structures in buffer solution (2). Atomic-scale resolution demonstrated on various solid–liquid interfaces (3) fosters hopes that the AFM may ultimately visualize structural changes of proteins which can be correlated with their biological activity. A first step to achieve this goal is the quantitative interpretation of the image. However, this is hindered by the limited understanding of image formation mechanisms. A quantitative comparison of AFM topographs with data from high-resolution electron microscopy is thus essential.

The system used for this study, the hexagonally packed intermediate (HPI) layer from the cell envelope of *Deinococcus radiodurans* is assembled from a single polypeptide of M_r 107,028 (4). Doughnut-shaped hexamers of M_r 655,000 (5) form a hexagonal lattice with unit cell dimensions $a = b = 18$ nm (6). This structure has three advantageous features for our experiment. (*i*) As it has been well characterized by electron microscopy, it permits one to evaluate the faithfulness of the image acquired by the AFM by a quantitative comparison at ≈1 nm resolution in all three dimensions. (*ii*) Composed of regularly arranged identical units, it allows a quantitative assessment of the resolution. (*iii*) As a two-dimensional lattice it is well suited for immobilization on a flat substrate, a prerequisite for imaging biological structures in aqueous solution with the AFM (7).

MATERIAL AND METHODS

HPI layer sheets from *D. radiodurans* (strain R1, ATCC 13939) were obtained by extraction of whole cells with sodium dodecyl sulfate and purified on a Percoll density gradient (8).

Immobilization of the HPI layer was achieved by a photocrosslinker that was covalently bound to a glass surface (7). Two microliters of the protein solution (1 mg/ml) was deposited on the chemically modified glass substrate, covered by a second glass plate, squeezed, and then irradiated for 3 min with a 366-nm 50-W light source. Images of immobilized HPI layers were recorded in 0.1 M phosphate buffer (pH 7.0) by a Nanoscope III AFM (Digital Instruments, Santa Barbara, CA). Silicon nitride cantilevers ($K = 0.38$ N/m; Digital Instruments) with a pyramidal stylus were used as purchased, the force applied to the stylus was 0.2–1 nN, and the scan speed was 300 nm/s.

For electron microscopy a small drop of 2% cadmium thioglycerol (9) was first applied to a carbon-coated grid made hydrophilic by glow-discharge. After 1 min, excess liquid was withdrawn and a small drop of the HPI layer suspension (1 mg/ml) was deposited. Sheets were allowed to adsorb for 1–2 min before most of the liquid was removed. Finally, another droplet of the cadmium thioglycerol solution was applied to ensure complete embedding of the specimen. All electron micrographs were recorded with a Philips EM 420 using low-dose procedures (9). Because cadmium thioglycerol is radiation-sensitive, the three-dimensional data set was collected over a tilt angle range between 0° and 80° in the form of many mini-tilt series, each of them comprising three to four micrographs, thus exposing the samples to a cumulative dose which was <4500 electrons per nm^2.

The Semper image-processing system was used to calculate correlation averages from AFM images and electron micrographs (10). Seventeen mini-tilt series were combined in performing the three-dimensional reconstruction. The micrographs were sorted into a "left-handed" and a "right-handed" data set corresponding to the two different orientations of the layer with respect to the supporting film; this differentiation was based on the handedness of the diffraction pattern. Identical areas within the mini-tilt series were digitized into 2048 by 2048 pixels of a size of 0.204 nm on the object by means of a Joyce–Loebl flat-bed densitometer. Correlation averages containing between 500 and 800 unit cells each were extracted from these projections. Effective tilt angle and tilt axis azimuth were evaluated from the base vectors of the projected lattices. Finally, the three-dimensional density distribution of the HPI layer was calculated from these data by aligning and normalizing individual projections, eliminating those that exhibited a correlation coefficient of <0.9 to neighboring projections (11). The two individual three-dimensional maps thus comprised 25 and 27 projections, respectively. The HPI hexamer was surface rendered at 100% mass by assuming a protein density of 810 Da/nm^3, and the topography of the side seen by the AFM was extracted.

For quantitative evaluation of the AFM data the averaged topography composed of 60 HPI hexamers was normalized to the layer thickness (7) and aligned with the topography of the HPI layer as obtained from electron microscopy to calculate the modulus of the difference. Further, the radial correlation function was determined from two independent averages to assess the lateral resolution (10), whereas the root-mean-

The publication costs of this article were defrayed in part by page charge payment. This article must therefore be hereby marked "*advertisement*" in accordance with 18 U.S.C. §1734 solely to indicate this fact.

Abbreviations: AFM, atomic force microscope; HPI layer, hexagonally packed intermediate layer.

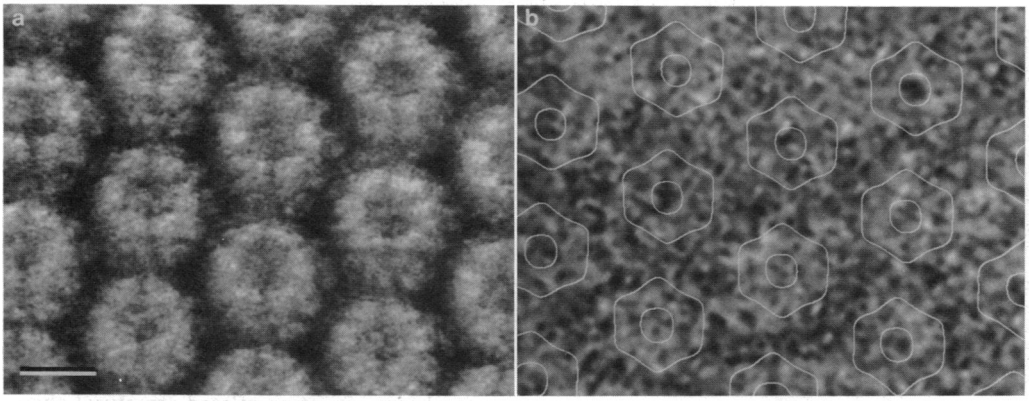

FIG. 1. HPI layer from the cell envelope of *D. radiodurans* in buffer solution as recorded by the AFM (*a*) and in cadmium thioglycerol as imaged by the electron microscope (*b*). To guide the eye, contours indicating the positions of HPI hexamers are superimposed on the electron micrograph. The gray-level range in *a* corresponds to 3 nm of vertical distance, and the scale bar represents 20 nm.

square (rms) deviation map computed from a stack of 50 aligned HPI hexamer topographs provided a measure for the reproducibility of the height values.

RESULTS AND DISCUSSION

Single HPI layers immobilized on a glass surface could be imaged with the AFM in buffer solution many times without significant structural deterioration when the force applied to the stylus was <1 nN (7). The scan displayed at a magnification of 8×10^5 in Fig. 1*a* shows the features of the HPI layer surface. One unit cell contains six morphological subunits that surround a central depression. Each subunit exhibits a V-shaped protrusion formed by two elongated structures, the "legs." The subunits are separated by clefts running approximately parallel to the lattice lines. Arms appear to emanate from this ring-shaped hexamer to provide connections to adjacent hexamers. A number of these features are distinct on most individual HPI unit cells of Fig. 1*a* even before elimination of the residual noise, whereas extensive image averaging is required to retrieve the structural information contained in a low-dose electron micrograph of an HPI layer (Fig. 1*b*).

To reduce the noise in the AFM image, ≈60 unit cells from four different scans recorded under conditions identical to those which apply to Fig. 1*a* were averaged by correlation methods (10). This averaged and sixfold rotationally symmetrized surface topograph is displayed as a three-dimensional view in Fig. 2*a*. For comparison, a three-dimensional density map of the HPI layer was reconstructed to a resolution of 1 nm by standard electron crystallographic methods (12)—i.e., by combining projection data recorded by the electron microscope. The extracellular surface of this map contoured to include 100% mass (Fig. 2*b*) is remarkably similar to the surface topograph recorded by the AFM, in terms of both the shape and the absolute heights. In fact, the difference map between these two surfaces plotted in Fig. 2*c* exhibits an average deviation of <0.5 nm. It reveals prominent differences on the connecting arms and at the tips of the V-shaped protrusions, whereas the main body of the protrusions is rather similar in both images. This suggests that the tip geometry is one factor that limits the quality of the image collected by the AFM: deviations from data obtained by electron microscopy occur mainly in deep trenches or on very fine structures. Indeed, the distinct asymmetry of the HPI hexamers in Fig. 1*a* must be related to the particular shape of the tip.

Our data allow the resolution of the AFM image of a protein surface in buffer solution to be assessed. First, the lateral resolution as determined by the radial correlation function between two independent averages (10) is ≈1.5 nm. This value represents an underestimate, because some features that can be clearly seen in the AFM topograph (Fig. 1*a*) are smaller. The legs of the V-shaped protrusions, for instance, have a width of 1.06 ± 0.1 nm (n = 18). This discrepancy indicates that the inherent flexibility of the sample allows for

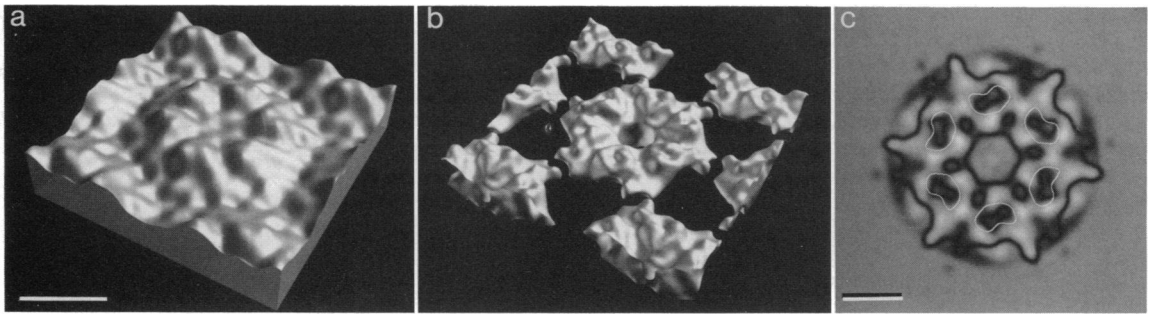

FIG. 2. Similarity between the averaged HPI topograph recorded by atomic force microscopy (*a*) and the surface-rendered three-dimensional map reconstructed from electron microscopic projections (*b*). In *c* the modulus of the difference between the average HPI topograph recorded by the AFM and the surface determined by the electron microscope is displayed. The gray-level range in *c* corresponds to 0.9 nm of vertical distance, and the scale bar represents 10 nm. Sixty HPI hexamers were averaged and sixfold symmetrized to produce the three-dimensional view in *a*. Projections were recorded in the electron microscope covering a tilt range up to +80°. Two independent data sets comprising 52 projections in total were combined to determine the structure factors along the lattice lines. The density map was contoured at 100% mass, and the extracellular surface was displayed in *b* under identical viewing conditions as the topograph shown in *a*. The difference map shown in *c* represents the modulus of the height difference between the aligned surfaces determined by the AFM and the electron microscope. Its average value is 0.44 nm, and peak values are close to 1 nm. The kidney-shaped contours mark the V-shaped protrusions as recorded with the AFM.

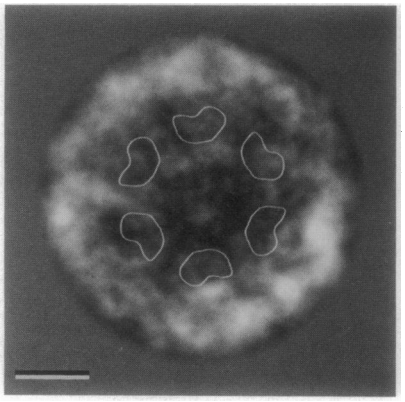

FIG. 3. Quantitative assessments of the AFM image reproducibility. The rms deviation map between individual HPI hexamer images recorded with the AFM exhibits small rms values in the center of the hexamer and maxima in the grooves between them. V-shaped protrusions are contoured with kidney-shaped outlines. Gray levels extend from 0-nm to 0.5-nm rms deviation and the scale bar represents 10 nm. To determine the rms deviation map, 50 HPI hexamers were extracted from HPI layer images and aligned angularly and translationally with respect to the average shown in Fig. 2*a*, and the rms deviation was calculated for each pixel. The average deviation amounts to 0.16 nm; minimum and maximum deviations are 0.05 nm and 0.47 nm, respectively.

some disorder that deteriorates the actual instrumental resolution. Second, an estimate of the vertical resolution is provided by the rms deviation of the height values between individual hexamer surfaces. The rms deviation map displayed in Fig. 3 has an average of 0.16 nm, and the minimum and maximum rms deviations are 0.05 nm and 0.47 nm, respectively. It was rather unexpected that the height measurements exhibit such a variable and position-dependent quality. Considering the slope of the V-shaped protrusions (≈0.5) and the rms values at their edges (≈0.1 nm), we estimate that the HPI hexamers are laterally aligned to better than 0.2 nm. Hence the pronounced fluctuations of the height values over the connecting arms between HPI hexamers are most likely not the result of lateral misalignment. Furthermore, the tip geometry would contribute to differences between images recorded by atomic force microscopy and by electron microscopy rather than variations within the AFM data. Therefore, the map appears to reflect the rigidity of the core structure; i.e., small rms values (0.05–0.1 nm) are measured on the V-shaped protrusions and in the center of the hexamer, whereas the largest errors are seen between hexamers (≈0.5 nm). This corroborates the impression gained by a closer examination of Fig. 1*a*: variations appear between the doughnut-shaped units rather than in their center or on the six prominent protrusions.

Images of the purple membrane (13), gap junction (14), and cholera toxin (15) have been recorded in buffer solution by atomic force microscopy. However, these images were not rigorously compared with structural data obtained by other methods. Here we demonstrate the quality and fidelity of AFM topographs by a quantitative comparison with data obtained by electron microscopy. The high resolution of these AFM topographs and their similarity to the data from electron microscopy are related to the use of a sharp stylus, imaging forces below 1 nN, and optimized scan speed, parameters that all need to be adjusted carefully. In addition, it appears that flexible regions can be discriminated from more rigid domains by evaluating the variations between images of many molecules. Thus, atomic force microscopy in physiological environments opens up interesting possibilities to assess the surface structure of biological membranes and other planar assemblies of biomacromolecules and possibly to observe function-related structural changes directly.

We thank Drs. U. Aebi, M. Dolder, R. Glaeser, J. P. Rosenbusch, and C. Schönenberger for critical discussions; U. Santarius for recording the mini-tilt series; and C. Henn for preparing the perspective views displayed in Fig. 2 with his program MAPVIEW. This work was supported by the Swiss National Foundation for Scientific Research (Grant 31-32536.91 to A.E.), the Research Foundations of Ciba-Geigy, Hoffmann–La Roche, and Sandoz, the M. E. Müller-Foundation of Switzerland, and the Deutsche Forschungsgemeinschaft (Grant Ba 618/6-3 to W.B.).

1. Binnig, G., Quate, C. F. & Gerber, C. (1986) *Phys. Rev. Lett.* **56**, 930–933.
2. Hoh, J. H. & Hansma, P. K. (1992) *Trends Cell Biol.* **2**, 208–213.
3. Manne, S., Butt, H. J., Gould, S. A. C. & Hansma, P. K. (1990) *Appl. Phys. Lett.* **56**, 1758–1759.
4. Peters, J., Peters, M., Lottspeich, F., Schäfer, W. & Baumeister, W. (1987) *J. Bacteriol.* **169**, 5216–5223.
5. Engel, A., Baumeister, W. & Saxton, W. O. (1982) *Proc. Natl. Acad. Sci. USA* **79**, 4050–4054.
6. Baumeister, W., Barth, M., Hegerl, R., Guckenberger, R., Hahn, M. & Saxton, W. O. (1986) *J. Mol. Biol.* **187**, 241–253.
7. Karrasch, S., Dolder, M., Schabert, F., Ramsden, J. & Engel, A. (1993) *Biophys. J.*, in press.
8. Baumeister, W., Karrenberg, F., Rachel, R., Engel, A., Ten Heggeler, B. & Saxton, W. O. (1982) *Eur. J. Biochem.* **125**, 535–544.
9. Jakubowski, U., Hegerl, R., Formanek, H., Volker, S., Santarius, U. & Baumeister, W. (1988) in *9th European Congress on Electron Microscopy York, England*, eds. Dickinson, H. G. & Goodhews, P. J. (Inst. of Phys., Bristol, U.K.), pp. 381–382.
10. Saxton, W. O. & Baumeister, W. (1982) *J. Microsc.* **127**, 127–138.
11. Saxton, W. O., Hahn, M. & Baumeister, W. (1984) *Ultramicroscopy* **13**, 57–70.
12. Henderson, R. & Unwin, P. N. T. (1975) *Nature (London)* **257**, 28–32.
13. Butt, H.-J., Downing, K. H. & Hansma, P. K. (1990) *Biophys. J.* **58**, 1473–1480.
14. Hoh, J. H., Sosinski, G. E., Revel, J.-P. & Hansma, P. K. (1993) *Biophys. J.* **65**, 149–163.
15. Yang, J., Tamm, L. K., Tillack, W. T. & Shao, Z. (1993) *J. Mol. Biol.* **229**, 286–290.